Sixth International Symposium on Marine Propulsors
smp'19, Rome, Italy, May 2019

Investigation of propeller cavitation using compressible large eddy simulations *

Mrugank Bhatt[1], **Krishnan Mahesh**[1]

[1]Department of Aerospace Engineering & Mechanics, University of Minnesota, Minneapolis, USA

ABSTRACT

Cavitation over a five bladed marine propeller (P4381) is studied using large eddy simulations (LES) at Reynolds number of 894,000 and advance ratio of 0.89. The simulations use the homogeneous mixture model, where the mixture of water and vapor is treated as a single compressible fluid. The numerical method of Gnanaskandan and Mahesh (2015) is extended to solve the governing equations in the rotating frame of reference using absolute velocity. Evaluation of propeller shaft orientation, numerical dissipation, pressure drop in vortex cores, freestream nuclei and grid resolution is presented. Simulations are performed for wetted conditions and thrust break down conditions. Propeller loads obtained from the simulations are compared to the experiments and flow field obtained using LES is used to analyse thrust breakdown.

Keywords LES, Propeller Cavitation, Thrust Breakdown.

1 INTRODUCTION

Cavitation is a major source of noise, structural vibrations and material damage on the marine propulsors. Cavitation limits the performance and efficieny of the propeller; and it can also lead to massive breakdown of thrust/torque. Hence, understanding the inception of cavitation, its development, and consequences to the flow field of propulsors is of importance.

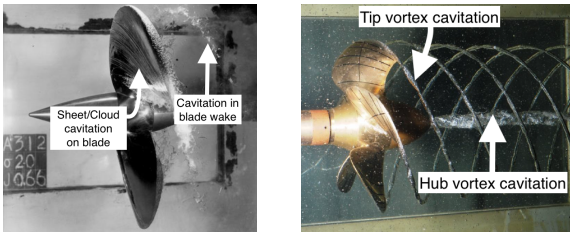

a) b)

Figure 1: Types of cavitation on marine propellers. a) Sheet/Cloud cavitation (Mitchell et al. (2013)) and b) vortex cavitation (Heinke (2011))

Recent numerical simulations of the single phase flow over marine propulsors have shown significant advancement. However, the same is not true for cavitating flows due to the following reasons. As shown in the figure 1, depending on the propeller geometry and the flow conditions multiple types of cavitation can co-exhist in the flow, such as vortex cavitation inside low pressure cores of tip and hub vortices, sheet/cloud type of cavitation on the suction side of the propeller blade similar to what is observed on hydrofoils. This results in a complex flow field of an inherently unsteady propeller wake. Also, it is known that as the flow cavitates, sound speed drops by orders of magnitude in the resulting water-vapor mixture as compared to nearly incompressible regions in water; presentinga wide range of Mach numbers in the flow. This requires accurate modeling of mixture compressibility, imposing time step restrictions due to resulting stiffness in the system. Finally, there exists a wide range of length/time scales due to both cavitation and turbulence, which requires accurate modeling of mass transfer and its interaction with turbulence.

In SMP-2015, a review of recent advances in both in-house and commercial solvers in predicting cavitation on marine propulsors has been published by Vaz et al. (2015) as a part of the Cooperative Reseach Ships SHARCS project. Numerical methods based on both RANS and coupled RANS–BEM (boundary element method) have been used to predict wetted and cavitating flows over propeller E779A. The study showed good agreement for propeller performance characteristics. Improvement however in predicting cavity extent and pressure fluctuations were deemed necessary. Bensow and Bark (2010) studied the flow over the same propeller using wall-modeled, implicit LES approach, and demonstrated the need for LES to capture detailed cavitation flow field for the prediction of cavitation erosion and noise.

Experimental flow over the open propeller P4381 for cavitation thrust/torque breakdown has been studied by Boswell (1971), which will be used for comparison of propeller performance. Numerically the configuration has been studied using the RANS methodology over a wide range of advance ratios by Lindau et al. (2005). Single phase flow over the same propeller using LES is studied by Kumar and Mahesh (2017). In the present work, we study experimental configuration using compressible LES under the wetted and thrust/torque breakdown conditions. Numerical method to solve turbulent cavitating flows using a homogeneous mixture approach developed by Gnanaskandan and Mahesh (2015) is extended to solve the governing equation in rotating frame of reference. Details aredescribed in section 2, along with the computa-

*Email for correspondence: kmahesh@umn.edu

tional grid, domain size and boundary conditions. Assessment of propeller shaft orientation, numerical dissipation, pressure drop in vortex cores, freestream nuclei and grid resolution are presented in 3 along with the analysis of wetted and thrust torque breakdown conditions of propeller.

2 SIMULATION DETAILS

2.1 Governing equations and numerical method

The simulations use the homogeneous mixture model, where the mixture of water and vapor is treated as a single compressible fluid. The mixture is assumed to be in thermodynamic and mechanical equilibruim among its constituent phases. The governing equations are the compressible Navier–Stokes equations solved for mixture quantities along with the transport equation for vapor mass transfer employing finite rate mass transfer between the phases. The equations are spatially Favre filtered for LES and given as;

$$\begin{aligned}
\frac{\partial \overline{\rho}}{\partial t} &= -\frac{\partial}{\partial x_k}\left(\overline{\rho}\tilde{u_k}\right), \\
\frac{\partial \overline{\rho}\tilde{u_i}}{\partial t} &= -\frac{\partial}{\partial x_k}\left(\overline{\rho}\tilde{u_i}\tilde{u_k} + \overline{p}\delta_{ik} - \tilde{\sigma}_{ik} - \tau_{ik}\right), \qquad (1) \\
\frac{\partial \overline{\rho}\tilde{Y}}{\partial t} &= -\frac{\partial}{\partial x_k}\left(\overline{\rho}\tilde{Y}\tilde{u_k} - t_k\right) + \tilde{S_e} - \tilde{S_c} \quad and \\
\frac{\partial \overline{\rho}\tilde{e_s}}{\partial t} &= -\frac{\partial}{\partial x_k}\left(\overline{\rho}\tilde{e_s}\tilde{u_k} - \tilde{Q_k} - q_k\right) \\
&\quad - \overline{p}\frac{\partial \tilde{u_k}}{\partial x_k} + \tilde{\sigma_{ik}}\frac{\partial \tilde{u_i}}{\partial x_k}.
\end{aligned}$$

Here, the tilde quantities are Favre averaged quantities and τ_{ik}, q_k and t_k are subgrid scale (SGS) terms namely: SGS stress, SGS heat flux and SGS scalar flux. These terms are modeled using the Dynamic Smagorinsky model (DSM) (Moin et al., 1991). ρ, u_i, e_s and p are density, velocity, internal energy and pressure respectively, of the mixture and Y is the vapor mass fraction. σ_{ij} and Q_{ij} are viscous stress tensor and heat flux vector respectively. S_e and S_c are evaporation and condensation source terms given by Saito et al. (2007). The system is closed by a non-barotropic mixture equation of state given by stiffened equation of state in water and ideal gas equation of state in vapor. The speed of sound of the mixture is derived from the mixture equation of state and the Gibbs equation, which compares well with measured frozen sound speed in literature.

The numerical method is based on a predictor-corrector approach, where the predictor step uses non-dissipative finite volume scheme and corrector step uses a characteristic based filter in the vicinity of discontinuities. Time integration is performed by the explicit Adams-Bashforth method. For detailed description of physical modeling and numerical methodology see Gnanaskandan and Mahesh (2015). The methodology has been successfully used to simulate multiple types of cavitation pertinent to propeller cavitation such as; sheet/cloud cavitation showing quantitative comparison for volume fraction for re-entrant jet (Gnanaskandan and Mahesh, 2016b) and condensation shock wave (Bhatt and Mahesh, 2018) induced transition; and vortex cavitation inside karman shedding over a cylinder (Gnanaskandan and Mahesh, 2016a). Hence, we only discuss extension of the methodology to achieve propeller rotation using rotating frame of reference.

2.2 Rotating frame of reference

Two popular approaches for rotation are : (i) relative velocity formulation and (ii) absolute velocity formulation. Relative velcity formulation involves easier implementation, but creates problems for larger domain sizes (such as used for propulsors) due to the high magnitudes of centrifugal source terms. Hence, we use absolute velocity formulation, which modifies the force balance in equation 1 as

$$\begin{aligned}
\frac{\partial \overline{\rho}\tilde{u_i}}{\partial t} &= -\frac{\partial}{\partial x_k}\left(\overline{\rho}\tilde{u_i}\tilde{u_k} + \overline{p}\delta_{ik} - \tilde{\sigma}_{ik} - \tau_{ik}\right) \qquad (2) \\
&\quad + \frac{\partial}{\partial x_k}\left(\overline{\rho}\tilde{u_i}\epsilon_{kjl}w_j x_l\right) + \rho\epsilon_{ijk}w_j u_{r_k}.
\end{aligned}$$

Here, w is angular velocity of rotating frame of reference. Absolute velocity u is related to the velocity in rotating reference frame (u_r) as $u = u_r + \epsilon_{ijk}w_j x_k$. Equation 2 is solved in rotating frame of reference in terms of absolute velocity, therefore it does not invole any contribution due to centrifugal force. This also simplifies the boundary condition implementation as it is now applied to absolute velocity directly. Note that this formulation adds additional contribution due to the Coriolis force and modifies the advection terms in the governing equations 1. Changes in the advection terms subsequently requires modification to the shock capturing of the method. Following the approach used by Economan (2014) in context of ALE, this additional contribution due to rotation indeed only changes the diagonal of the jacobian matrix, which can be fit into the existing framework of the code.

2.2.1 Validation

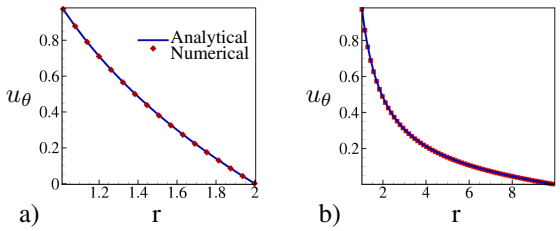

Figure 2: Comparison with analytical solution of Taylor-Couette flow for a) smaller and b) extended domain sizes.

The extension to the rotating frame of reference is validated using the Taylor-Couette problem for two different domain sizes based on the outer radius. $R_i = 1m$ and $R_o = 2m, 10m$ (smaller and extended domains) are radius of inner and the outer cylinder respectively. Outer cylinder is kept stationary in either cases (angular velocity $w_o = 0$) and the inner cylinder is rotated at angular velocity $w_i = 1rad/s$, mimicking the radial domain for propeller shaft rotation without axial velocities. Numerical results for radial variation of azimuthal velocity profiles are compared to analytical solution showing good agreement

for both smaller and extended domain sizes in figure 2.

2.3 Computational grid and boundary conditions

The entire computational domain along with a closer view of hub/shaft orientation and corresponding experimental configuration is illustrated in figure 3. The domain is a cylinder of diameter $7.0D$ and length $5.5D$, where D is the diameter of the propeller disk. The co-ordinate system is oriented such that the positive x axis is along the flow direction. Free stream velocities are prescribed at inflow and farfield lateral boundaries. Pressure is prescribed at the outflow in order to match the cavitation number $\sigma = \frac{p-p_v}{0.5\rho U^2}$, where p_v is vapor pressure, ρ and U are free stream density and velocity respectively. No-slip boundary conditions are prescribed on the walls. The blades and hub rotate with $U = w \times r$, and the shaft is stationary as shown in figure 3(b). Angular velocity w is prescribed in order to match the advance ratio, defined as $J = \frac{U}{nD}$, where n is the rotation rate. In order to avoid reflections of pressure waves from the boundaries back into the domain, we apply accoustically absorbing sponge layer spanning a distance of D at inflow, outflow and farfield boundaries. This adds additional term in the governing equations given by, $\Gamma(q-q_{ref})$ (Colonius, 2004). Here 'q' denotes the vector of conservative variables and the subscript 'ref' denotes the reference solution to which the flow is damped to, which is free stream values in the cases considered. 'Γ' denotes the amplitude of the forcing.

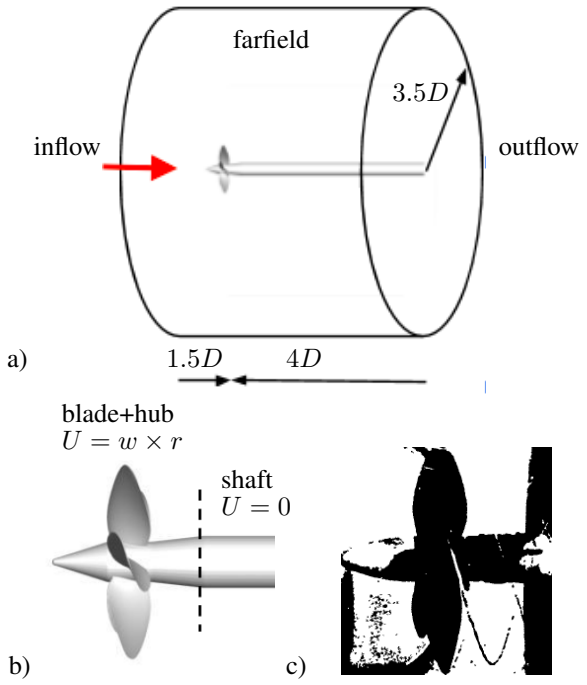

Figure 3: a) Complete domain for simulations. b) Closer view of blade, hub and shaft orientation. c) Experimental configuration of Boswell (1971) showing $\sigma = 1.4$

In addition, the grid is coarsened in the far field to further reduce any reflections. The unstructured grid for the propeller is shown in figure 4. Here we consider two different grid sizes $grid1$ and $grid2$, consisting of 11,532,735 and 21,422,580 hexahederal control volumes. The grid is clustered close to the solid surfaces; $grid2$ has a minimum wall-normal spacing of $0.0017D$ on blade, hub and shaft surfaces. The grids remain finer in the near wake of the propeller and are subsequently coarsened along both axial and radial directions. Blade wake consists of approximately 250 cells along axial direction past blade, 110 cells in the radial direction spanning the blade tip, total 300 cells in the azimuthal direction.

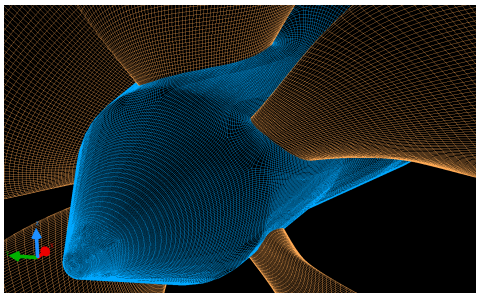

Figure 4: Surface mesh near blade and hub.

3 RESULTS

Flow is simulated over a marine propeller P4381 at design advance ratio, $J = 0.89$ at a Reynolds number, $Re = 894,000$. The geometric details of the propeller P4381 are reported in Boswell (1971). Reynolds number is defined based on the diameter of propeller disk as $Re = \frac{UD}{\nu}$. The notation used for propeller performance through out the paper is as follows. Thrust T is the axial component of force and torque Q is axial component of the moment of force. Non-dimensional thrust coefficient is defined as $K_T = \frac{T}{\rho n^2 D^4}$ and torque coefficient is defined as $K_Q = \frac{Q}{\rho n^2 D^5}$. Wetted conditions are simulated at high σ (referred to as $\sigma = \infty$ suggesting non-cavitating conditions) and thrust/breakdown case is considered at $\sigma = 0.6$.

3.1 Initialization

In compressible flow solvers, regions of non-zero flow divergence lead to the formation of pressure waves. Due to the sudden start of the propeller, strong compression waves are formed which propagate in the entire domain. In such case it is undesirable as it not only affects the stability of the solver but also elongates the simulation time due to transients. Hence, in order to prescribe divergence free initial conditions for the cavitation solver, the solution is first obtained using in-house incompressible flow solver MPCUGLES (Mahesh et al. (2004)) at given Re and J.

Table 1: Comparison of propeller performance with change of hub/shaft orientation.

	K_T	K_Q
Kumar and Mahesh (2017)	0.21	0.041
hub/shaft flipped	0.22	0.041

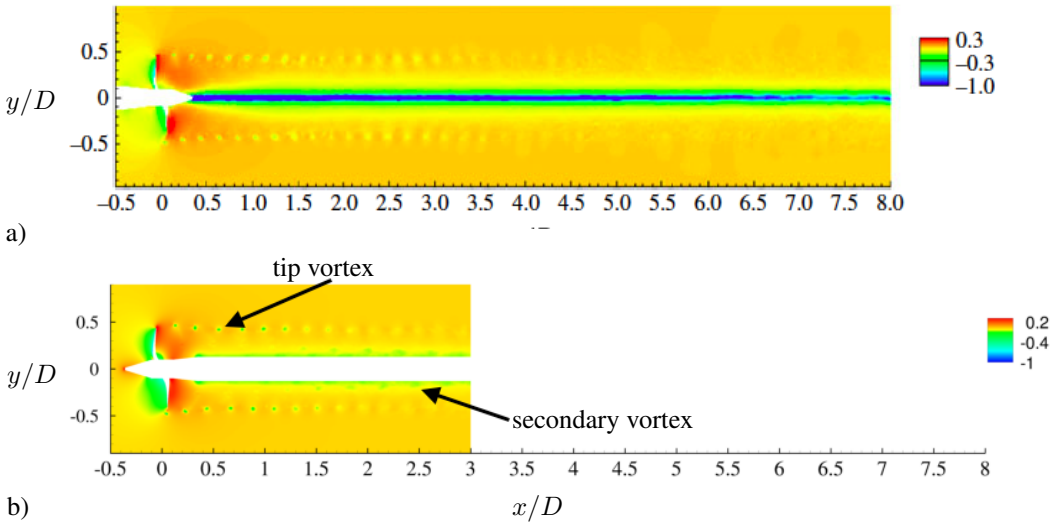

Figure 5: Instantaneous pressure field in the xy plane at $z = 0$. a) Kumar and Mahesh (2017) and b) current.

Detailed analysis of single phase flow at the same $Re = 894,000$ and $J = 0.89$ using MPCUGLES is considered by Kumar and Mahesh (2017). In the present work, we match the experimental configuration of Boswell (1971) as shown in figure 3(c), accordingly the direction of hub/shaft is flipped as compared to the original configuration studied by Kumar and Mahesh (2017). Instantaneous pressure field in the propeller wake for both configuration is compared in figure 5. It is noted that when the hub/shaft is flipped, in the absence of hub vortex, vorticity completes itself in the form of secondary vortices near the shaft as shown in figure 5(b). Comparison of propeller loads obtained using MPCUGLES for both the configuration is tabulated in 1, suggesting that orientation of hub/shaft has only nominal effect on overall forces. Torque in particular is not affected due to the lower moment arm of hub/shaft.

3.2 Wetted conditions

The cavitation code is initialized with the velocity field obtained using MPCUGLES, and pressure is prescribed corresponding to the given cavitation number(σ). Here we present the results for the propeller in forward mode under wetted conditions on Boswell (1971) configuration. The nature of instantaneous solution is illustrated by iso-contours of axial vorticity as shown in figure 6. Coherent vortical structures are evident in the tip vortices along with shedding of vorticity near blade trailing edge and in the boundary layer on the shaft. Instantaneous flow field in the wake past the propeller blade is visualized by considering the axial velocity profiles in $x - y$ plane at $z = 0$ as shown in figure 4. Near field is dominated by coherent tip vortics (also evident from 6) and the blade trailing edge wake. As one moves downstream beyond $1.0D$ pockets of blade wake become indistinguisable due to the breaking up of coherent structures in the near field resulting in flow turbulence and mixing.

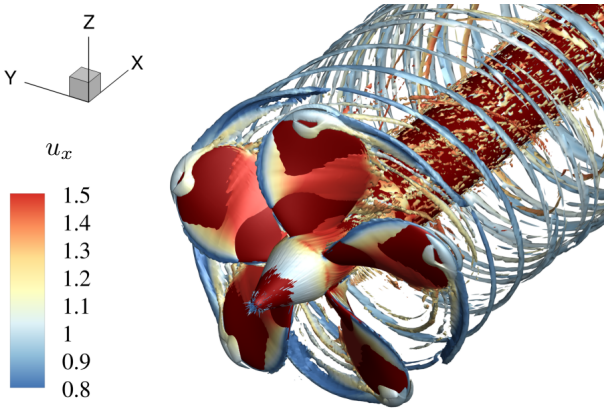

Figure 6: Isocontours of axial vorticity colored by u_x.

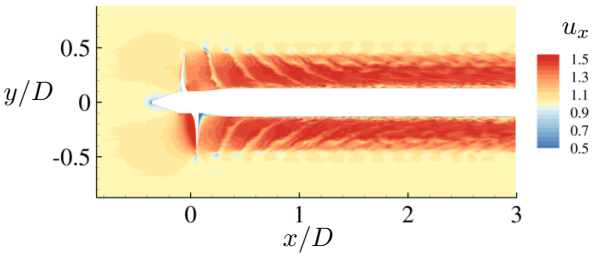

Figure 7: Instantaneous solution showing axial velocity.

Comparison of propeller performance obtained from LES with that of Boswell (1971) is presented in table 2, showing good agreement in thrust coefficient and 10% deviation in computed and experimental toque coefficient.

Table 2: Comparison of propeller performance under wetted conditions.

	K_T	K_Q
Boswell (1971)	0.215	0.045
LES	0.226	0.050

3.2.1 Shock capturing

First, we assess the sensitivity of propeller performance to the shock capturing scheme. As described in section 1, methodology is based on predictor-corrector approach, where predictor step does not explicitly add dissipation and hence in order to capture discontinuites (both shocks and material discontinuity), fluxes are corrected using characteristic based filtering approach where filtered numerical fluxes (i.e. corrected fluxes) are of the following form

$$F^*_{fc} = k\frac{1}{2}R_{fc}\theta_{fc}\phi_{fc}. \quad (1)$$

Here, F_{fc} represents corrected flux, R_{fc} is the right eigenvector vector at the face computed using Roe-average of the variables from left and right control volumes. θ_{fc} is the Harten's switch function and ϕ_{fc} has the Harten-Yee TVD form with minmod limiter; see Gnanaskandan and Mahesh (2015) for details.

Here, k is an adjustable parameter. The value of k is problem dependent and its effects on the results is demonstrated by Gnanaskandan and Mahesh (2015) and recommended values for a given type of problem is provided by Yee et al. (1999). In brief, extremely small values of k implies negligible dissipation which can lead to oscillations in the solution, whereas larger values lead to dissipation of small scales. In context of this problem we asses this by considering $k = 1.5$ and $k = 5$. As shown in table 3, the chosen values of k do not have significant effect on overall propeller performance except for nominal increase in thrust/torque for $k = 1.5$.

Table 3: Sensitivity of propeller performance with shock capturing

	K_T	K_Q
k=5	0.244	0.054
k=1.5	0.257	0.055

Next, we assess the effect of k on the local flow features particulary of interest such as tip vortices. Figure 8(a) displays phase average mean pressure field subtracted from free stream pressure obtained for $k = 1.5$. Pressure extracted along the line passing through the series of tip vortices in the propeller wake as indicated in figure 8(a) is plotted in figure 8(b). Here, we assess the pressure drop inside vortex cores obtained using incompressible solution (MPCUGLES), cavitation solver with k=1.5 and k=5. It is observed that as one travels downstream along the propeller wake, the pressure drop inside tip vortices decreases subsequently. It is noted that minor variations in this trend are expected due to the slip stream in the propeller wake, as a result the extracted line at few locations does not pass exactly through the vortex center. Here, the motivation for including incompressible solution for comparison is bifold; pressure drop from incompressible solution is often used as an indicator to find possible regions of cavitation inception, and in addition to that it also provides the baseline for non-dissipative solution in order to assess solution obtained using shock capturing. It is observed that at lower k (i.e. at $k = 1.5$) closer comparison to MPCUGLES is obtained. This suggest that although the shock capturing does not have significant effect on overall propeller performance, in order to capture local flow features accurately an appropriate assessment is necessary.

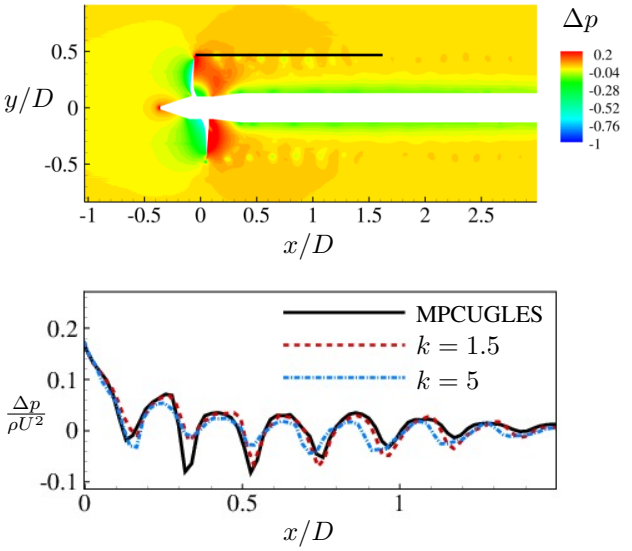

Figure 8: a) Phase averaged mean pressure for k=1.5. b) pressure drop along the line extracted at $r = D$ from $x = 0$ to $x = 1.5D$ as indicated in part(a).

3.2.2 Grid resolution

Here, we assess the sensitivity of propeller performance to grid resolution. Table 4 shows thrust/torque obtained using $grid1$ and $grid2$ (grid sizes as described in section 3), indicating that propeller performance is independent of the grid sizes used.

Table 4: Grid convergence

	K_T	K_Q
$grid1$	0.257	0.055
$grid2$	0.261	0.056

Figure 9 shows instantaneous pressure drop inside vortex cores for two different grids. It is plotted by extracting line passing through tip vortices as shown in figure 8(a). Note that grids considered here have nearly uniform spacing in the axial, radial and azimuthal direction in the propeller

wake. Axial location of pressure minimum for both the cases are identical upto $0.5D$, however the with finer grid lower values of pressure minimum are observed. Beyond $0.5D$ the identical values of minimum pressure is observed.

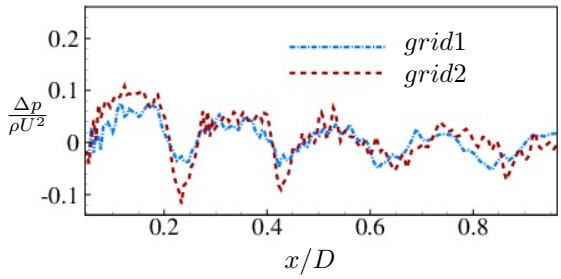

Figure 9: Instantaneous pressure drop along the line extracted at $r = D$ from $x = 0$ to $x = 1.5D$.

3.2.3 Effect of free stream nuclei

At a pressure lower than the vapor pressure, cavitation is triggered by imperfections in water, that are mostly small non-condensable gas or vapor bubbles (known as cavitation nuclei) and are the starting point for the liquid breakdown Franc and Michel (2005). Although these nuclei are usually present in any hydrodynamic system and often unavoidable, their amount and distribution is often not characterized or reported.

In the homogeneous mixture model, these cavitation nuclei are typically prescribed by considering certain amount of vapor/gas volume fraction through inflow and as initial condition inside the domain. In the present work, we consider three different values of free stream volume fraction (α_∞) 0.1, 0.01 and 0.0001. Standard value of α_∞ as denoted in the original mass transfer model by Saito et al. (2007) is 0.001. However, experimental measurements on background nuclei concentration suggest much lower values.

Table 5: Propeller performance with variation in nuclei concentration

	K_T	K_Q
α_∞=0.1	0.278	0.065
α_∞=0.01	0.257	0.055
α_∞=0.0001	0.226	0.050
Boswell (1971)	0.215	0.045

We assess the sensitivity of the propeller performance with free stream nuclei concentration as tabulated in 5. It is interesting to note that the forces acting on the propeller are sensitive to the free stream nuclei. It is evident that with the reduction in α_∞, propeller performance compare closer to the experiments, smallest value of $\alpha_\infty = 0.0001$ showing closest comparison. This indicate that under wetted conditions (i.e. under non-cavitating conditions), flow is quite sensitive to the amount of background nuclei. Consequently, for predicting cavitation inception, characterization of cavitation nuclei and its appropriate adaptation in numerical simulations is important.

Sound speed of the compressible homogeneous mixture is sensitive to the small amount of vapor volume fraction in the cell. Changes in α_∞ considered here leads to nearly order of magnitude changes in the sound speed; e.g. $101m/s$ for $\alpha_\infty = 0.01$ to $828m/s$ for $\alpha_\infty = 0.0001$, with lowering of α_∞ sound speed tends toward liquid. Consequently, Mach numbers in the free stream reduces significantly with lowering of α_∞, resulting in stiff system due to the large ratio of the acoustic and convective time scales (Turkel, 1987). Non-dimensional time step ($\bar{t} = tU/D$) used for calculations at $\alpha_\infty = 0.1$ of 4×10^{-5}, reduces to 2×10^{-6} at $\alpha_\infty = .0001$.

3.3 Thrust/torque breakdown

Here, we consider a case at $\sigma = 0.6$. Note that these calculations are performed for original configuration used by Kumar and Mahesh (2017) for single phase flows, and hence the hub/shaft is upstream of propeller compared to Boswell (1971) experiment. The solution obtained using a coarse grid of approximately 2 million hexahedral cell is presented here. Results for $\sigma = 0.6$ is compared to wetted case simulated for the same configuration and mesh size.

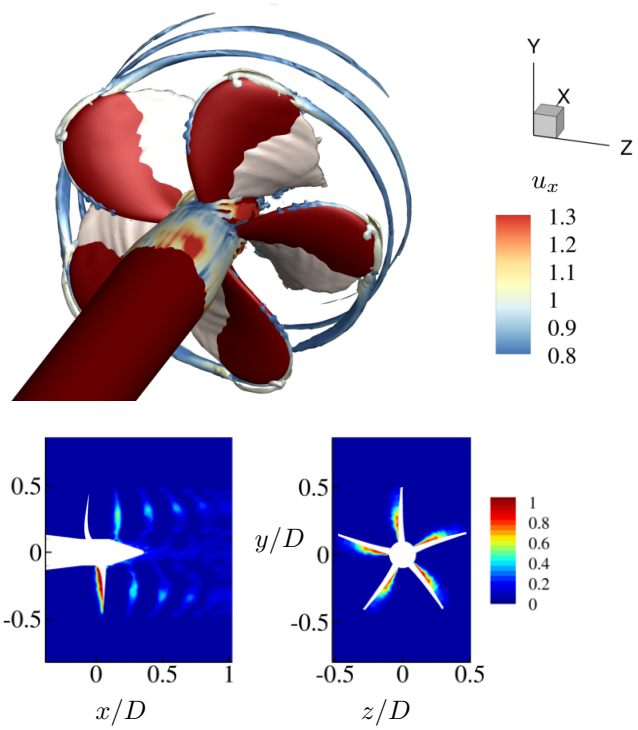

Figure 10: Propeller cavitation at $\sigma = 0.6$. a) Instantaneous solution showing i) iso-contours for $\alpha = 0.5$ and ii) iso-contours of axial vorticity colored by u_x. b) α in $x - y$ plane for $z = 0$. c) α in $y - z$ plane for $x = 0$.

Cavitation at $\sigma = 0.6$ is visualized using instantaneous solution for vapor volume fraction with $\alpha = 0.5$ iso-contours as shown in figure 10(a). It is observed that cavity sheet forms spanning the entire radial extent of the suction side

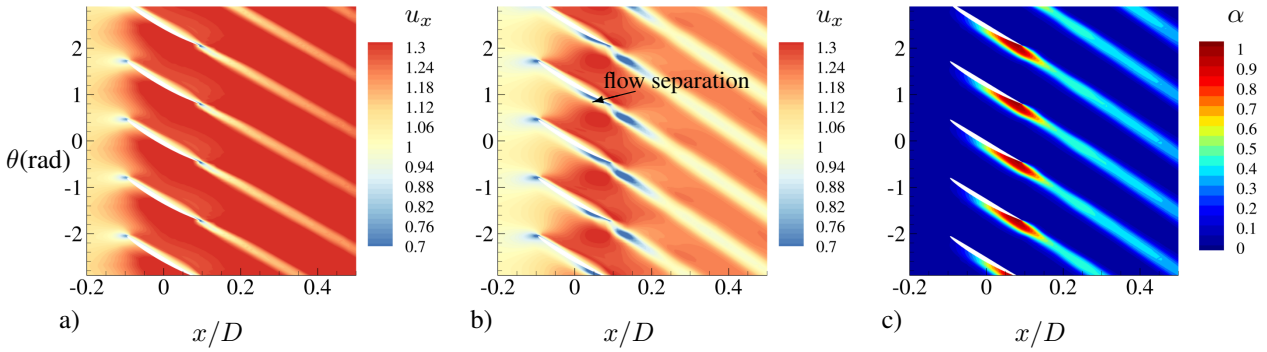

Figure 11: Flow inside blade passages for azimuthal plane at maximum propeller loading $r = 0.6D$. a) u_x for $\sigma = \infty$, b) u_x for $\sigma = 0.6$ and c) α for $\sigma = 0.6$.

of blade. Iso-contours of axial vorticity are used to indicate that no cavitation is observed inside the coherent vortices at the tip. This is expected as maximum propeller loading for P4381 is approximately at $r = 0.6D$ and reduces significantly as one travel radially outward towards the tip. For the details of load distribution see Kumar and Mahesh (2017). Axial cut-plane for α as shown in figure 10(b) indicate the presence of vapor pockets in the blade wake although with smaller values of vapor volume fractions ($\alpha < 0.5$). Radial cut-plane at blade center ($x = 0$) shows that vapor is more concentrated towards center and root of the blade.

Propeller performance obtained at $\sigma = 0.6$ is compared to the wetted case as tabulated in 6. Overall performance of propeller shows massive reduction in thrust and torque at $\sigma = 0.6$. Considering the use of coarse grid for this configuration here, actual quantitative values for propeller performance are only preliminary.

Table 6: Propeller performance breakdown due to cavitation

	K_T	K_Q
$\sigma = \infty$	0.18	0.038
$\sigma = 0.6$	0.077	0.021

3.3.1 Explanation for thrust/torque breakdown due to cavitation

We consider the influence of cavition on the general flow field inside blade passeges and near wake of propeller. In order to assess the effect of cavitation, we compare the results to the wetted case. Figure 11 shows flow inside blade passage for azimuthal plane at $r = 0.6D$ corresponding to the location of maximum propeller loading. We see that in the wetted case, flow accelerates in the blade passage and remains attached to the blade suction side as shown in figure 11(a) by red contour regions of phase averaged axial velocity profiles. This results in overall increase in momentum past propeller blades and consequently production of thrust. Although this is not the case at $\sigma = 0.6$ as shown in figure 11(b). It is observed that flow acceleration is much smaller and in fact flow separates after the mid chord as indicated by blue contour regions. This can be explained by considering the α distribution inside blade passages as shown in figure 11(c). The regions of flow separation in figure 11(b), correlates to the vapor formation on blade suction side. In summary, as the pressure drops on blade suction side flow accelerates passing through the blade passage; however, if the pressure drops below vapor pressure the flow cavitates, which in turn leads to flow separation. Hence, overall increase in momentum past propeller is significantly reduced and consequently the performance of propeller.

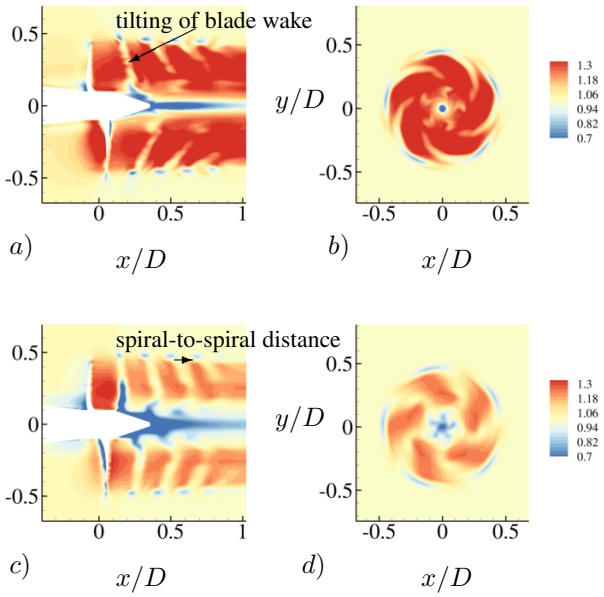

Figure 12: Phase averaged axial velocity profiles in near wake of propeller illustrated using; a) $x-y$ plane at $z = 0$ for $\sigma = \infty$, b) $y-z$ plane at $x = 0.5D$ for $\sigma = \infty$, c) $x-y$ plane at $z = 0$ for $\sigma = 0.6$ and d) $y-z$ plane at $x = 0.5D$ for $\sigma = 0.6$.

As illustrated in figure 11(b), in case of $\sigma = 0.6$, thicker strips indicating negligible flow acceleration are observed

in the flow advected downstream in the propeller near wake. Axial velocity contours in the near wake of propeller is illustrated by figure 12. These strips are also noticeable when near wake of propeller is visualized using $x-y$ plane as shown in figure 12(c). It is evident that flow acceleration is significantly reduced past the blades of propeller when compared to wetted case as showin in 12(a). Figure 12(b,d) shows comparison in $y-z$ plane at a distance $x = 0.5D$ in propeller wake. At $\sigma = 0.6$ larger radial extent near the hub shows negligible flow acceleration. Comparing figures 12(a,b), it is interesting to note that tilting of the blade wake is significantly reduced at $\sigma = 0.6$ as a result of lower gain in momentum as compared to wetted conditions. In addition to that, at $\sigma = 0.6$, the distance between the tip vortices is also reduced. In case of single phase flow Kumar and Mahesh (2017) observed that the mutual inductance between the rolled up trailing edge wake and the tip vortices dominated the evolution of propeller wake from the near field to far field. In presence of cavitation, as a result of reduction in spiral-to-spiral distance between tip vortices and reduction in blade wake tilting this interaction is expected to be affected.

4 SUMMARY

In the present work, flow over a five bladed marine propeller (P4381) is investigated at design advance ratio under wetted and thrust/torque breakdown conditions using LES. Mixture of water-vapor is modeled as a single compressible fluid using a homogeneous mixture approach and compressible Navier-Stokes equations are applied to the mixture quantities. Methodology is extended to solve governing equations in rotating frame of reference using absolute velocity formulation to achieve propeller rotation.

An important aspect of initializing the compressible flow solver is considered. A divergence free initial condition necessary to avoid transient pressure waves generated due to the sudden start of propeller is provided using in-house incompressible flow solver MPCUGLES (Mahesh et al. (2004)). In order to match the experimental configuration of Boswell (1971), orientation of hub/shaft is flipped as compared to the configuration used by Kumar and Mahesh (2017). Change of orientation of hub/shaft showed only nominal effect on overall propeller performance.

Wetted flow conditions are simulated at Re=894,000 and J=0.89. Effect of shock capturing is assessed by adjusting the corrector fluxes to the non-dissipative predictor step. No significant effect of numerical dissipation is observed on the propeller performance for the considered corrector fluxes. Propeller performance obtained using LES is shown to be independent of grids considered. However, a finer grid resolution and lower numerical dissipation enabled better capturing of minimum pressure inside tip vortex cores. It was interesting to note that under wetted conditions, flow showed sensitivity to the amount of background nuclei. A parameteric study performed over a range of free stream nuclei showed closest comparison to experiments for the lowest value of free stream nuclei considered.

Thrust/torque breakdown is studied for $\sigma = 0.6$. Massive cavitation is observed spanning entire radial extent of the suction side of the blade and continuing along the wake with pockets of low void fraction. Overall thrust/torque droped by more than a factor of 2 as compared to wetted case. Breakdown of thrust/torque is explained by considering significant reduction in momentum gain through propeller blades as a result of flow separation at blade suction. Cavitation led to the lowering of spiral-to-spiral distance between tip vortices and reduction in blade wake tilting; as a result influencing the wake instability.

ACKNOWLEDGEMENTS

This work is supported by the United States Office of Naval Research under Grant ONR N00014-14-1-0290 and ONR N00014-17-1-2676 with Dr. Ki-Han Kim as the program manager. The computations were made possible through the computing resources provided by the U.S. Army Engineer Research and Development Center (ERDC) in Vicksburg, Mississippi on the machines copper and onyx of High Performance Computing Modernization program (HPCMP).

REFERENCES

Bensow, R. E. and Bark, G. "Implicit LES predictions of the cavitating flow on a propeller". Journal of Fluids Engineering, 132, 2010.

Bhatt, M. and Mahesh, K. "Investigation of sheet to cloud transition due to the propagation of condensation fronts over a sharp wedge using large eddy simulations". 10th International symposium on cavitation, 2018.

Boswell, R. J. "Design, cavitation performance, and open-water performance of a series of research skewed propellers". Report : Naval ship research and development center Washington, D.C., 1971.

Colonius, T. "Modeling artificial boundary conditions for compressible flow". Ann. Rev. Fluid Mech, 36:315–345, 2004.

Economan, T. D. "Optimal shape design using an unsteady continuous adjoint approach". PhD Dissertation, 2014.

Franc, J.P and Michel, J.M. In Fundamentals of Cavitation. 2005.

Gnanaskandan, A. and Mahesh, K. "A numerical method to simulate turbulent cavitating flows". International Journal of Multiphase Flows, 70:22–34, 2015.

Gnanaskandan, A. and Mahesh, K. "Numerical investigation of near-wake characteristics of cavitating flow over a circular cylinder". J. Fluid Mech, 790:453–491, 2016a.

Gnanaskandan, A. and Mahesh, K. "Large eddy simulation of the transition from sheet to cloud cavitation over a wedge". Intl. J. Multiphase Flows, 83:86–102, 2016b.

Heinke, H-J. "Potsdam propeller test case (PPTC)- cavitation test case 2.3". Second International Sysmposium on Marine Propulsors, 2011.

Kumar, P. and Mahesh, K. "Large eddy simulation of pro-

peller wake instabilities". Journal of Fluid Mechanics, 814:361–396, 2017.

Lindau, J. W., Boger, D. A., Medvitz, R. B., and Kunz, R. F. "Propeller cavitation breakdown analysis". Journal of Fluids Engineering, 127, 2005.

Mahesh, K., Constantinescu, G., and Moin, P. "A numerical method for large–eddy simulation in complex geometries". Journal of Computational Physics, 197:1: 215, 2004.

Mitchell, G.H.G., Sampson, R., and Atlar, M. "A modern approach to the representation and use of the kca systematic propeller series". Third International Symposium on Marine Propulsors, 2013.

Moin, P., Squires, K., Cabot, W., and Lele, S. "A dynamic subgrid-scale model for compressible turbulence and scalar transport". Physics of Fluids, 3(11):2746–2757, 1991.

Saito, Y., Takami, R., Nakamori, I., and Ikohagi, T. "Numerical analysis of unsteady behavior of cloud cavitation around a NACA0015 foil.". Comp. Mech, 40:85–96, 2007.

Turkel, E. "Preconditioned methods for solving the incompressible and low speed compressible equations". Journal of Computational Physics, 72:277–298, 1987.

Vaz, G., Hally, D., Huuva, Tobias, Bulten, Norbert, Muller, Pol, Becchi, Paolo, Herrer, J. L. R., Whitworth, S., Mace, R., and Korsstrom, A. "Cavitating flow calculations for the E779A propeller in open water and behind conditions: Code comparison and solution validation". Fifth International Symposium of Marine Propulsors, 2015.

Yee, Helen C, Sandham, Neil D, and Djomehri, MJ. "Low-dissipative high-order shock-capturing methods using characteristic-based filters". Journal of Computational Physics, 150(1):199–238, 1999.